Cite as: Y. Chu *et al.*, *Science* 10.1126/science.aao1511 (2017).

Quantum acoustics with superconducting qubits

Yiwen Chu,*[1,2] Prashanta Kharel,[1,2] William H. Renninger,[1,2] Luke D. Burkhart,[1,2] Luigi Frunzio,[1,2] Peter T. Rakich,[1,2] Robert J. Schoelkopf*[1,2]

[1]Department of Applied Physics, Yale University, New Haven, CT 06511, USA. [2]Yale Quantum Institute, Yale University, New Haven, CT 06520, USA.
*Corresponding author. Email: yiwen.chu@yale.edu (Y.C.); robert.schoelkopf@yale.edu (R.J.S.)

Mechanical objects have important practical applications in the fields of quantum information and metrology as quantum memories or transducers for measuring and connecting different types of quantum systems. The field of electromechanics is in pursuit of a robust and highly coherent device that couples motion to nonlinear quantum objects such as superconducting qubits. Here, we experimentally demonstrate a high-frequency bulk acoustic wave resonator that is strongly coupled to a superconducting qubit using piezoelectric transduction with a cooperativity of 260. We measure qubit and mechanical coherence times on the order of 10 microseconds. Our device requires only simple fabrication methods and provides controllable access to a multitude of phonon modes. We demonstrate quantum control and measurement on gigahertz phonons at the single quantum level.

Measuring and controlling the motion of massive objects in the quantum regime is of great interest for both technological applications and for furthering our understanding of quantum mechanics in complex systems. However, it remains an open question whether macroscopic mechanical objects can be engineered, controlled, and utilized in ways analogous to what has been demonstrated in cavity (*1*) or circuit QED (*2*). By addressing this question, we may be able to use mechanical systems as powerful resources for quantum information and metrology, such as universal transducers or quantum memories that are more compact than their electromagnetic counterparts (*3*–*6*). In addition, since any coupling of qubits to other degrees of freedom can lead to decoherence, it is crucial to understand and control the interaction qubits might have to their mechanical environments (*7*).

In the field of quantum electro-mechanics, there has been a variety of experimental efforts to couple mechanical motion to superconducting circuits. The majority of demonstrations have involved megahertz frequency micromechanical oscillators parametrically coupled to gigahertz frequency electromagnetic resonators in the linearized interaction regime (*8*, *9*). Because both electrical and mechanical modes are linear, these systems only allow for the generation of Gaussian states of mechanical motion. Alternatively, the creation of useful non-Gaussian states, including Fock states or Schrödinger cat states, requires a source of quantum nonlinearity, which can be introduced through a qubit (*10*, *11*) or obtained in the yet-unexplored regime of a strong nonlinear coupling (*4*).

Demonstrations of mechanics coupled to superconducting qubits include interactions with propagating surface acoustic waves (*12*) and micromechanical resonators in both the dispersive (*13*) and resonant (*14*, *15*) regimes. A central goal of these experiments is to reach the regime of quantum acoustics, in which the ability to make, manipulate, and measure non-classical states of light in cavity or circuit QED becomes applicable to mechanical degrees of freedom. This regime requires the strong coupling limit, where the coupling strength g is much larger than the loss rates of the qubit and the oscillator. Piezoelectric materials are natural choices for achieving large coupling strengths between single electrical and mechanical excitations (*11*, *16*). Nevertheless, there has only been one proof-of-principle demonstration of a nonlinear electromechanical system in the strong coupling limit (*15*). However, this groundbreaking device has not yet lead to further developments in quantum acoustics due to the complexity of its fabrication and relatively low cooperativity. Therefore, the search continues for a robust and easily implemented electromechanical system with sufficient coherence and coupling strengths to allow for higher fidelity and more complex quantum operations (*12*, *16*).

In this Report, we address this important challenge by experimentally demonstrating strong coupling between a superconducting qubit and the phonon modes of a high-overtone bulk acoustic wave resonator (HBAR). The system incorporates a piezoelectric transducer into a standard 3D transmon geometry (*17*). By performing basic quantum operations with the qubit, we reach the mechanical ground state and measure long coherence times (>10 μs) of single phonons. The cooperativity of our system is 260, comparable to that of early circuit QED devices (*18*) and more than an order of magnitude higher than the previous strongly coupled qubit-mechanical system (*15*). This dramatic improvement in cooperativity is due to three orders of magni-

Downloaded from http://science.sciencemag.org/ on September 21, 2017

tude increase in coherence times of both the qubit and mechanics. In addition, we demonstrate the unique feature of many high-Q phonon modes that are all individually addressable by the qubit.

Our quantum electromechanical device, shown in Fig. 1A, consists of a frequency-tunable aluminum transmon coupled to phonons in its non-piezoelectric sapphire substrate using a thin disk of c-axis oriented aluminum nitride (AlN) (*19*). The top surface of the AlN film and the bottom surface of the sapphire form a phononic Fabry-Perot resonator that supports longitudinally polarized thickness modes (see Fig. 1B), which are well studied in the context of conventional HBAR technologies (*20*). The piezoelectricity of the AlN generates stress $\ddot{\sigma}(\vec{x})$ from the transmon's electric field $\vec{E}(\vec{x})$, which acts on the phonon modes's strain field $\ddot{s}(\vec{x})$. For simplicity, we consider only the dominant tensor components $E \equiv E_3$, $\sigma \equiv \sigma_{33}$, $s \equiv s_{33}$, where the subscript *3* denotes the longitudinal direction perpendicular to the substrate surface. Then the interaction energy between the transmon and the phonon mode is given by $H = -\int \sigma(\vec{x}) s(\vec{x}) dV$, where $\sigma(\vec{x}) = c_{33} d_{33}(\vec{x}) E(\vec{x})$ and c_{33} and d_{33} are the stiffness and piezoelectric tensor components, respectively. Quantizing the fields and equating this to the Jaynes-Cummings Hamiltonian, we can estimate the coupling strength as $\hbar g = c_{33} \int d_{33}(\vec{x}) E(\vec{x}) s(\vec{x}) dV$ [see (*19*) for details].

Having described the physics of the electromechanical coupling, we now introduce a simple picture that captures the essential character of the acoustic modes and allows us to estimate coupling rates and mode frequencies. Because the acoustic wavelength is much smaller than the diameter of the AlN disk, the transduced acoustic waves do not diffract significantly and remain inside the cylindrical volume of sapphire underneath the AlN for a relatively long time. The spatial character and frequencies of the phonons can be approximated by considering the stationary modes $s_{l,m}(\vec{x})$ of this cylindrical mode volume, which are illustrated in Fig. 1B and described in (*19*). According to this simplified model, the transmon couples to discrete modes with distinct longitudinal (l) and transverse (m) mode numbers. For example, the l = 503, m = 0 phonon mode has a frequency of ~6.65 GHz. We can obtain $E(\vec{x})$ from electromagnetic simulations of a transmon at that frequency and estimate the coupling strength g to be on the order of $2\pi \times 300$ kHz.

Another important consideration for reaching the strong coupling limit is the mechanical loss, which we expect to be dominated by diffraction out of the finite mode volume into the semi-infinite sapphire substrate. To estimate this loss, we consider a second model in which the transmon couples to the semi-continuous set of lossless modes of a much larger volume. The coherent temporal evolution of these modes will conspire to reproduce the diffraction loss of the original strain profile. As shown in (*19*), we use this method to estimate the phonon's diffraction limited lifetime to be on the order of many microseconds, indicating that our system should be in the strong coupling regime.

We see from these descriptions that the modes of our mechanical system are physically very different from that of micromechanical resonators (*13*, *15*). We will show that, despite diffraction loss, our system has a much higher quality factor than micromechanical resonators at the same frequency (*15*). In addition, a greater fraction of the mechanical energy in our system resides in an almost perfect crystal rather than in potentially lossy interfaces and surfaces (*5*). Combined with the lack of complex fabrication processes that could further increase material dissipation, we expect our system to be a path toward very low loss mechanical resonators.

We now turn to experiments that showcase the power of the above principles in creating a coupled qubit-phonon device with drastically improved performance. The mechanically coupled qubit is placed inside a copper rectangular 3D cavity at v_c = 9.16 GHz with externally attached flux tuning coils. This device is mounted on the base plate of a dilution refrigerator and measured using standard dispersive readout techniques with a Josephson parametric converter amplifier (*21*).

By performing spectroscopy on the qubit, which consists of the transmon's lowest two energy levels *g* and *e*, we are able to observe the hallmarks of strong coupling to the modes of the HBAR. As we vary the qubit frequency with applied flux, we observe a series of evenly spaced anticrossings, which are consistent with phonons of different longitudinal mode numbers (Fig. 2A). These anticrossings occur every $v_{FSR} = v_l/2h$ = 13.2 MHz as we tune the transmon's frequency by over a gigahertz [see (*19*)]. For a measured substrate thickness of 420 μm, v_{FSR} corresponds to the free spectral range (FSR) of a HBAR with longitudinal sound velocity $v_l = 1.11 \times 10^4$ m/s, which agrees well with previously measured values for sapphire. More detailed spectroscopy data around a single longitudinal mode reveals additional weaker anticrossings, shown in Fig. 2B and the inset to Fig. 2A. These features reproduce for all nine longitudinal modes we investigated and are due to qubit coupling to modes $s_{l,m}(\vec{x})$ with the same l and different m. We also observe the effect of these modes when we excite the qubit and measure its state after variable delay (Fig. 2C). Far away from the anticrossing point, we measure an exponential decay corresponding to a qubit lifetime of T_1 = 6 μs. Around the anticrossing, we observe clear evidence of vacuum Rabi

Downloaded from http://science.sciencemag.org/ on September 21, 2017

oscillations. The oscillations are distorted on the lower current (higher qubit frequency) side due to the presence of $m = 1$ mode, and there are additional details associated with weakly coupled higher m modes. As shown in (*19*), by simulating the experiments in Fig. 2, B and C using the first four transverse mode numbers, we find good agreement with the data and extract a coupling constant for the $m = 0$ mode of $g = 2\pi \times (260 \pm 10)$ kHz, which agrees reasonably well with our prediction of $2\pi \times 300$ kHz.

We now show that the electromechanical coupling can be used to perform coherent quantum operations on the qubit-phonon system. While we will focus on a single longitudinal mode from here on, we point out that the following demonstrations can be performed with any of the observed longitudinal modes, which are all individually addressable by the qubit. The qubit's interaction with each phonon mode can controlled by tuning it on and off resonance with that mode. To perform useful quantum operations this way, the tuning must be performed over a frequency range much larger than g and on a timescale much faster than one vacuum Rabi oscillation period. This is difficult to achieve using flux tuning, but can be accomplished by Stark shifting the qubit with an additional microwave drive (*22*). We first flux tune the qubit to ω_b indicated in Fig. 2B. To avoid coupling to the higher order transverse modes, we apply a drive 100 MHz detuned from the microwave cavity with a constant amplitude that Stark shifts the qubit to ω_{or}. This is the off resonant frequency of the qubit where it can be controlled and measured as an uncoupled transmon. Decreasing the Stark shift amplitude makes the qubit resonant with the phonons and allows for energy exchange.

To calibrate the Stark shift control, we reproduce the vacuum Rabi oscillations shown in Fig. 3C using a pulsed Stark drive. From this data, we can determine an amplitude and length of the pulse, indicated by a white cross in Fig. 3A, that transfers a single electromagnetic excitation of the nonlinear transmon into a mechanical excitation of the phonon and vice versa. We note here that, in principle, this swap operation transfers the qubit state into a superposition of phonons with different transverse mode numbers. However, it mainly populates the one phonon Fock state of the $m = 0$ mode.

We first use our ability to perform operations on the qubit-phonon system to show that the mechanical oscillator is in the quantum ground state. We find that the transmon has a ground state population of 92% (Fig. 3B). Ideally, the transmon and phonon should be in their ground states since both are in the regime of $k_B T \ll \hbar\omega$. If we first perform a swap operation between the qubit and phonon, we find that the transmon's ground state population increases to 98%. This value is likely limited by the fidelity of the swap operation and therefore represents a lower bound on the phonon ground state population. This result indicates that the phonons are indeed cooled to the quantum ground state, in fact more so than the transmon. The swap operation can be used to increase the transmon polarization with the phonon mode, which can also be seen in an increased contrast of g-e Rabi oscillations (Fig. 3C).

To further verify that our system is indeed in the strong coupling regime, we now present measurements of the phonon's coherence properties. To measure the phonon T_1, we excite the qubit and then perform two swap operations with a variable delay in between (Fig. 4A). We find that the resulting qubit excited state population is well described by an exponential decay with a time constant of $T_1 = 17 \pm 1$ μs with the addition of a decaying sinusoid with frequency of $2\pi \times (340 \pm 10)$ kHz, which is due to interference between the $m = 0$ and $m = 1$ modes. This T_1 is in qualitative agreement with our predictions of the diffraction limited lifetime and gives a phonon quality factor of $Q = 7.1 \times 10^5$. We also measure a phonon T_2 decoherence time between the vacuum and one phonon Fock state of 27 ± 1 μs using a modified Ramsey sequence (Fig. 4B).

The results presented here are the first demonstrations of an electromechanical system with significant room for improvement. There are clear paths toward enhancing both the coherence and interaction strength of the system to bring it further into the strong coupling regime. The most obvious improvement is to increase the transmon T_1, which is currently the limiting lifetime in the system. 3D transmons with $T_1 \sim 100$ μs have been demonstrated on sapphire, and measured values for the tan δ of AlN (*23*) suggest that the transmon T_1 is not currently limited by additional dielectric loss in the transducer. Another significant improvement would be to modify the geometry so that the transmon couples more strongly to a longer-lived phonon mode with a single transverse mode number. This can be done by shaping the surfaces of the substrate to create a stable phonon resonator with transverse confinement (*24*, *25*). The AlN transducer can also be made with a curved profile to minimize higher spatial Fourier components of the piezoelectric drive (*26*).

These improvements will open up possibilities for more sophisticated quantum acoustics demonstrations in the future. With stronger coupling and lower loss, we can treat the phonons analogously to the modes of an electromagnetic resonator. For example, with tools that we have already demonstrated, we will be able to create and read out higher phonon Fock states (*27*). With the appropriate detuning between the qubit and phonon, it may be possible to reach the strong dispersive regime or directly excite the phonons with a microwave drive. The combination of these abilities will allow us to create highly non-classical mechanical states such as Schrodinger cat states, which may be useful for

Downloaded from http://science.sciencemag.org/ on September 21, 2017

probing the boundary between quantum and classical systems (*28*). At the same time, large quality factors of up to ~10^8 have been demonstrated in bulk acoustic waves resonators (*16*, *24*, *25*) which is comparable to the longest lived 3D superconducting cavities. However, phonons may offer distinct advantages over photons as a quantum resource in cQED devices. For example, due to the difference in the speed of sound and light, the HBAR has a much smaller mode volume that supports a large number of longitudinal modes that can all be coupled to the qubit, resulting in a multimode register for the storage of quantum information. Such straightforward individual accessibility to a collection of phononic quantum modes is unique to the geometry of our device and is not possible in most micromechanical resonators. In addition, our results indicate that phonon radiation could be a loss mechanism for superconducting circuits if piezoelectric materials are present (*7*). Finally, bulk acoustic waves have been shown to couple to a variety of other quantum mechanical objects ranging from infrared photons to solid state defects (*24*, *29*). Therefore, our device presents new possibilities for microwave to optical conversion and transduction in hybrid quantum systems.

REFERENCES AND NOTES

1. A. Reiserer, G. Rempe, Cavity-based quantum networks with single atoms and optical photons. *Rev. Mod. Phys.* **87**, 1379–1418 (2015). doi:10.1103/RevModPhys.87.1379
2. C. Wang, Y. Y. Gao, P. Reinhold, R. W. Heeres, N. Ofek, K. Chou, C. Axline, M. Reagor, J. Blumoff, K. M. Sliwa, L. Frunzio, S. M. Girvin, L. Jiang, M. Mirrahimi, M. H. Devoret, R. J. Schoelkopf, A Schrödinger cat living in two boxes. *Science* **352**, 1087–1091 (2016). doi:10.1126/science.aaf2941 Medline
3. M. J. A. Schuetz, E. M. Kessler, G. Giedke, L. M. K. Vandersypen, M. D. Lukin, J. I. Cirac, Universal quantum transducers based on surface acoustic waves. *Phys. Rev. X* **5**, 031031 (2015). doi:10.1103/PhysRevX.5.031031
4. M. Aspelmeyer, T. J. Kippenberg, F. Marquardt, Cavity optomechanics. *Rev. Mod. Phys.* **86**, 1391–1452 (2014). doi:10.1103/RevModPhys.86.1391
5. M. Poot, H. S. van der Zant, Mechanical systems in the quantum regime. *Phys. Rep.* **511**, 273–335 (2012). doi:10.1016/j.physrep.2011.12.004
6. J. Bochmann, A. Vainsencher, D. D. Awschalom, A. N. Cleland, Nanomechanical coupling between microwave and optical photons. *Nat. Phys.* **9**, 712–716 (2013). doi:10.1038/nphys2748
7. L. B. Ioffe, V. B. Geshkenbein, Ch. Helm, G. Blatter, Decoherence in superconducting quantum bits by phonon radiation. *Phys. Rev. Lett.* **93**, 057001 (2004). doi:10.1103/PhysRevLett.93.057001 Medline
8. J. B. Clark, F. Lecocq, R. W. Simmonds, J. Aumentado, J. D. Teufel, Sideband cooling beyond the quantum backaction limit with squeezed light. *Nature* **541**, 191–195 (2017). doi:10.1038/nature20604 Medline
9. J. M. Fink, M. Kalaee, A. Pitanti, R. Norte, L. Heinzle, M. Davanço, K. Srinivasan, O. Painter, Quantum electromechanics on silicon nitride nanomembranes. *Nat. Commun.* **7**, 12396 (2016). doi:10.1038/ncomms12396 Medline
10. A. D. Armour, M. P. Blencowe, K. C. Schwab, Entanglement and decoherence of a micromechanical resonator via coupling to a Cooper-pair box. *Phys. Rev. Lett.* **88**, 148301 (2002). doi:10.1103/PhysRevLett.88.148301 Medline
11. A. N. Cleland, M. R. Geller, Superconducting qubit storage and entanglement with nanomechanical resonators. *Phys. Rev. Lett.* **93**, 070501 (2004). doi:10.1103/PhysRevLett.93.070501 Medline
12. M. V. Gustafsson, T. Aref, A. F. Kockum, M. K. Ekström, G. Johansson, P. Delsing, Propagating phonons coupled to an artificial atom. *Science* **346**, 207–211 (2014). doi:10.1126/science.1257219 Medline
13. M. D. LaHaye, J. Suh, P. M. Echternach, K. C. Schwab, M. L. Roukes, Nanomechanical measurements of a superconducting qubit. *Nature* **459**, 960–964 (2009). doi:10.1038/nature08093 Medline
14. F. Rouxinol, Y. Hao, F. Brito, A. O. Caldeira, E. K. Irish, M. D. LaHaye, Measurements of nanoresonator-qubit interactions in a hybrid quantum electromechanical system. *Nanotechnology* **27**, 364003 (2016). doi:10.1088/0957-4484/27/36/364003 Medline
15. A. D. O'Connell, M. Hofheinz, M. Ansmann, R. C. Bialczak, M. Lenander, E. Lucero, M. Neeley, D. Sank, H. Wang, M. Weides, J. Wenner, J. M. Martinis, A. N. Cleland, Quantum ground state and single-phonon control of a mechanical resonator. *Nature* **464**, 697–703 (2010). doi:10.1038/nature08967 Medline
16. X. Han, C.-L. Zou, H. X. Tang, Multimode strong coupling in superconducting cavity piezoelectromechanics. *Phys. Rev. Lett.* **117**, 123603 (2016). doi:10.1103/PhysRevLett.117.123603 Medline
17. H. Paik, D. I. Schuster, L. S. Bishop, G. Kirchmair, G. Catelani, A. P. Sears, B. R. Johnson, M. J. Reagor, L. Frunzio, L. I. Glazman, S. M. Girvin, M. H. Devoret, R. J. Schoelkopf, Observation of high coherence in Josephson junction qubits measured in a three-dimensional circuit QED architecture. *Phys. Rev. Lett.* **107**, 240501 (2011). doi:10.1103/PhysRevLett.107.240501 Medline
18. A. Wallraff, D. I. Schuster, A. Blais, L. Frunzio, R. Huang, J. Majer, S. Kumar, S. M. Girvin, R. J. Schoelkopf, Strong coupling of a single photon to a superconducting qubit using circuit quantum electrodynamics. *Nature* **431**, 162–167 (2004). doi:10.1038/nature02851 Medline
19. See the supplementary materials.
20. K.-Y. Hashimoto, *RF Bulk Acoustic Wave Filters for Communications* (Artech House, 2009).
21. B. Abdo, F. Schackert, M. Hatridge, C. Rigetti, M. Devoret, Josephson amplifier for qubit readout. *Appl. Phys. Lett.* **99**, 162506 (2011). doi:10.1063/1.3653473
22. Z. Leghtas, S. Touzard, I. M. Pop, A. Kou, B. Vlastakis, A. Petrenko, K. M. Sliwa, A. Narla, S. Shankar, M. J. Hatridge, M. Reagor, L. Frunzio, R. J. Schoelkopf, M. Mirrahimi, M. H. Devoret, Confining the state of light to a quantum manifold by engineered two-photon loss. *Science* **347**, 853–857 (2015). doi:10.1126/science.aaa2085 Medline
23. A. D. O'Connell, M. Ansmann, R. C. Bialczak, M. Hofheinz, N. Katz, E. Lucero, C. McKenney, M. Neeley, H. Wang, E. M. Weig, A. N. Cleland, J. M. Martinis, Microwave dielectric loss at single photon energies and millikelvin temperatures. *Appl. Phys. Lett.* **92**, 112903 (2008). doi:10.1063/1.2898887
24. W. H. Renninger, P. Kharel, R. O. Behunin, P. T. Rakich, Bulk crystalline optomechanics, *arXiv:1703.08231* (2017).
25. S. Galliou, M. Goryachev, R. Bourquin, P. Abbé, J. P. Aubry, M. E. Tobar, Extremely low loss phonon-trapping cryogenic acoustic cavities for future physical experiments. *Sci. Rep.* **3**, 2132 (2013). doi:10.1038/srep02132 Medline
26. S.-H. Park, H. Jeon, Y.-J. Sung, G.-Y. Yeom, Refractive sapphire microlenses fabricated by chlorine-based inductively coupled plasma etching. *Appl. Opt.* **40**, 3698–3702 (2001). doi:10.1364/AO.40.003698 Medline
27. M. Hofheinz, H. Wang, M. Ansmann, R. C. Bialczak, E. Lucero, M. Neeley, A. D. O'Connell, D. Sank, J. Wenner, J. M. Martinis, A. N. Cleland, Synthesizing arbitrary quantum states in a superconducting resonator. *Nature* **459**, 546–549 (2009). doi:10.1038/nature08005 Medline
28. S. Nimmrichter, K. Hornberger, Macroscopicity of mechanical quantum superposition states. *Phys. Rev. Lett.* **110**, 160403 (2013). doi:10.1103/PhysRevLett.110.160403 Medline
29. E. R. MacQuarrie, T. A. Gosavi, N. R. Jungwirth, S. A. Bhave, G. D. Fuchs, Mechanical spin control of nitrogen-vacancy centers in diamond. *Phys. Rev. Lett.* **111**, 227602 (2013). doi:10.1103/PhysRevLett.111.227602 Medline
30. L. S. Bishop, J. M. Chow, J. Koch, A. A. Houck, M. H. Devoret, E. Thuneberg, S. M. Girvin, R. J. Schoelkopf, Nonlinear response of the vacuum Rabi resonance. *Nat. Phys.* **5**, 105–109 (2008). doi:10.1038/nphys1154
31. K. Geerlings, Z. Leghtas, I. M. Pop, S. Shankar, L. Frunzio, R. J. Schoelkopf, M. Mirrahimi, M. H. Devoret, Demonstrating a driven reset protocol for a superconducting qubit. *Phys. Rev. Lett.* **110**, 120501 (2013). doi:10.1103/PhysRevLett.110.120501 Medline
32. C. Wang, C. Axline, Y. Y. Gao, T. Brecht, Y. Chu, L. Frunzio, M. H. Devoret, R. J. Schoelkopf, Surface participation and dielectric loss in superconducting qubits. *Appl. Phys. Lett.* **107**, 162601 (2015). doi:10.1063/1.4934486

Downloaded from http://science.sciencemag.org/ on September 21, 2017

33. J. Koch, T. M. Yu, J. Gambetta, A. A. Houck, D. I. Schuster, J. Majer, A. Blais, M. H. Devoret, S. M. Girvin, R. J. Schoelkopf, Charge-insensitive qubit design derived from the cooper pair box. *Phys. Rev. A* **76**, 042319 (2007). doi:10.1103/PhysRevA.76.042319
34. J. Johansson, P. Nation, F. Nori, Qutip: An open-source python framework for the dynamics of open quantum systems. *Comput. Phys. Commun.* **183**, 1760–1772 (2012). doi:10.1016/j.cpc.2012.02.021
35. A. Fox, T. Li, Computation of optical resonator modes by the method of resonance excitation. *IEEE J. Quantum Electron.* **4**, 460–465 (1968). doi:10.1109/JQE.1968.1075368

ACKNOWLEDGMENTS

We thank M. Devoret, K. Lehnert, H. Tang, and H. Jung for helpful discussions. We thank K. Silwa for providing the Josephson parametric converter amplifier. This research was supported by the U.S. Army Research Office (W911NF-14-1-0011). Facilities use was supported by the Yale SEAS cleanroom, the Yale Institute for Nanoscience and Quantum Engineering (YINQE), and the NSF (MRSEC DMR 1119826). L.D.B acknowledges support from the ARO QuaCGR Fellowship. R.J.S. and L.F. are founders and equity shareholders of Quantum Circuits, Inc. All authors are inventors on patent application no. 62/465,101 submitted by Yale University, which covers Techniques for Coupling Qubits to Acoustic Resonators and Related Systems and Methods.

SUPPLEMENTARY MATERIALS

www.sciencemag.org/cgi/content/full/science.aao1511/DC1
Materials and Methods
Supplementary Text
Figs. S1 to S8
References (*32*–*35*)

25 June 2017; accepted 5 September 2017
Published online 21 September 2017
10.1126/science.aao1511

Downloaded from http://science.sciencemag.org/ on September 21, 2017

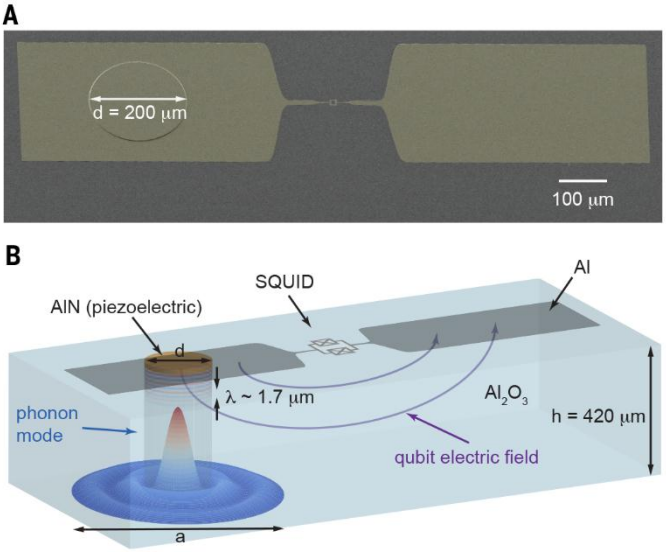

Fig. 1. Qubit with piezoelectric transducer. (A) False color SEM image of a transmon qubit on a sapphire substrate with one electrode covering an AlN transducer, which is ~900 nm thick and *d* = 200 μm in diameter. (B). Schematic of piezoelectric coupling to the modes of a HBAR (not to scale). The longitudinal part of the wave function is illustrated by a sinusoidal profile with wavelength $\lambda = 2h/l$ on the cylindrical mode volume defined by the AlN disk and the sapphire substrate underneath. The transverse energy density profile of $s_{l,0}(\vec{x})$ is plotted in 3D, showing the effective confinement of energy inside the mode volume, while some energy leaks out due to diffraction. This also illustrates that the $s_{l,0}(\vec{x})$ mode corresponds to the $s'_{l,3}(\vec{x})$ mode of a larger volume with diameter *a*.

Downloaded from http://science.sciencemag.org/ on September 21, 2017

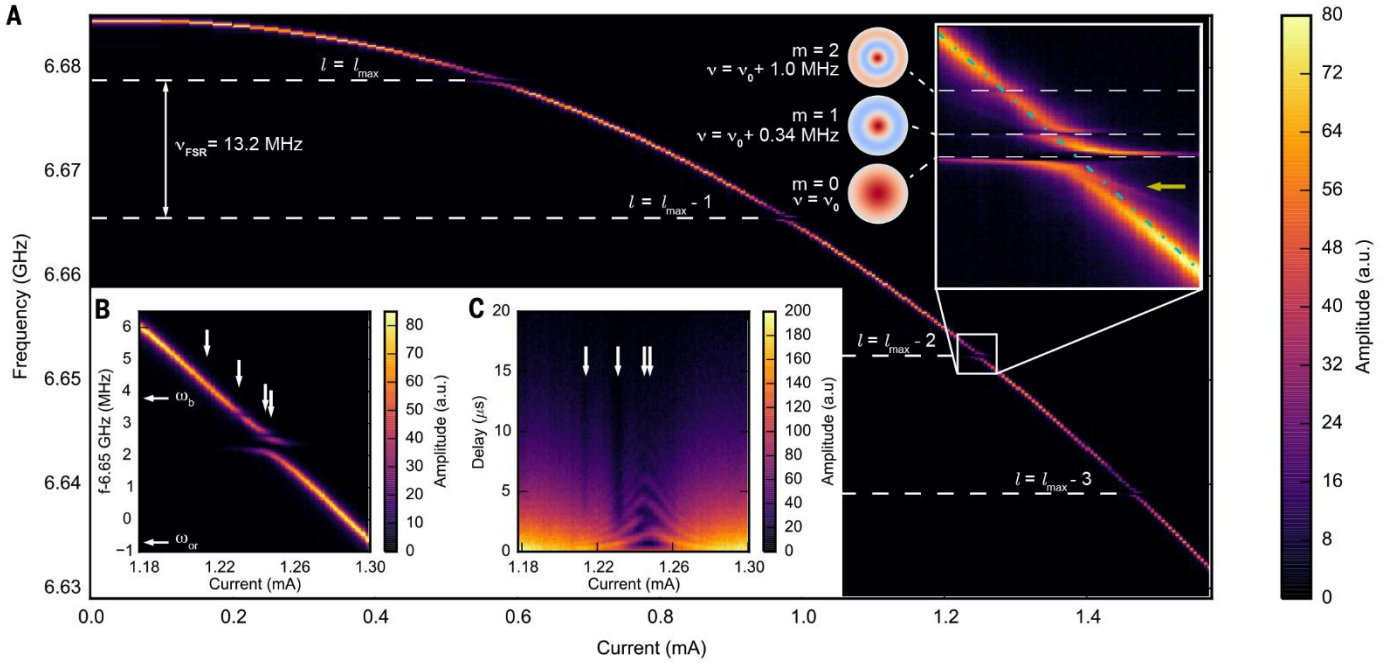

Fig. 2. Spectroscopy of qubit-phonon coupling. (A) Qubit spectroscopy as a function of current applied to flux tuning coil. White dashed lines indicate anticrossings for different longitudinal wavenumbers. The highest accessible longitudinal mode is l_{max} = 505, assuming v_l is constant with frequency. (Inset) Detailed spectroscopy around the l = 503 anticrossing, which is also used in (B) and (C), along with Figs. 3 and 4. Blue dash-dot line shows the frequency of the uncoupled qubit. Dashed white lines indicate anticrossings for m = 0,1,2, whose transverse mode profiles are plotted to the left. The frequencies of these modes are given relative to ν_0 = 6.65235 GHz. The faint feature indicated by a yellow arrow is due to multiphoton transitions to higher states of the Jaynes-Cummings level structure (*30*). (B and C) Spectroscopy and qubit dynamics. Vertical arrows indicate locations of prominent subfeatures. Horizontal arrows in (B) indicate frequencies used for Stark shift control, as described in the text. In (C), the qubit excitation pulse is 20 ns long, which ensures that the bandwidth is large enough to excite the hybridized qubit-phonon states.

Downloaded from http://science.sciencemag.org/ on September 21, 2017

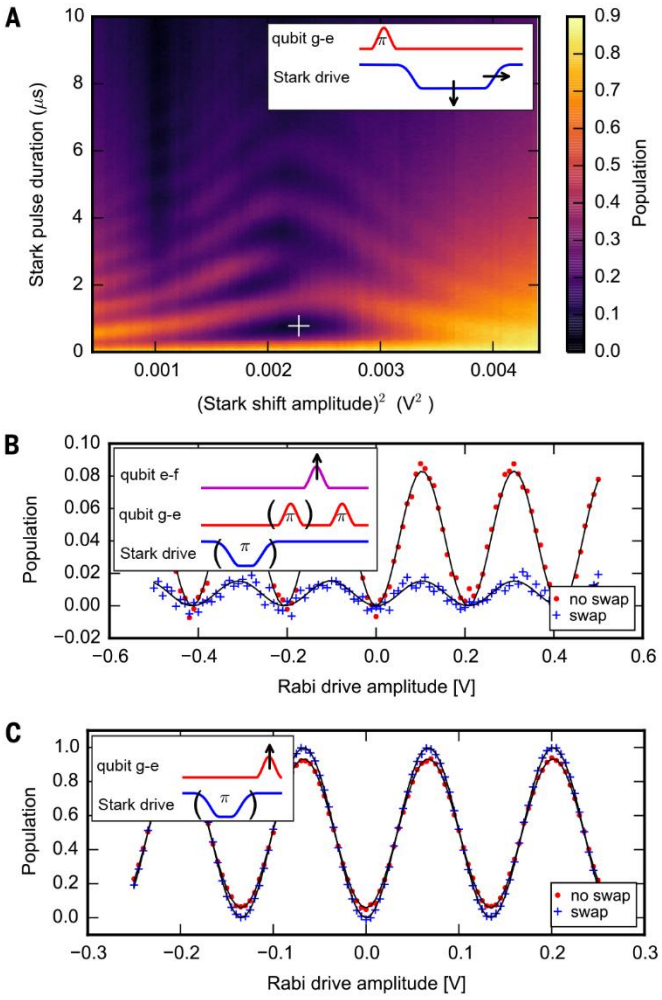

Fig. 3. Quantum control of the qubit-phonon system. (A) Vacuum Rabi oscillations measured by varying the amplitude and duration of the Stark drive pulse after exciting the qubit while it is off resonant from the phonons, as shown in the inset. The pulse is a decrease in the Stark drive amplitude with a rise time of 50 ns. Except for Fig. 3B, axes labeled "Population" in Figs. 3 and 4 correspond to all populations not in the g state. (B) Measurement of the excited state populations of the qubit and phonon. We plot measured Rabi oscillations between the e state and the transmon's third energy level *f*, normalized using the same experiment with a preceding g-e π pulse [see (*19*, *31*) for details]. The amplitude of oscillations gives the population in the $n = 1$ Fock state of the phonon or the e state of the qubit, depending on whether or not a swap operation is performed at the beginning. Black lines show sinusoidal fits to the data. (C) Rabi oscillations between the g and e qubit states, with and without a preceding swap operation. We use the former to calibrate the qubit population measurements in Figs. 3 and 4.

Downloaded from http://science.sciencemag.org/ on September 21, 2017

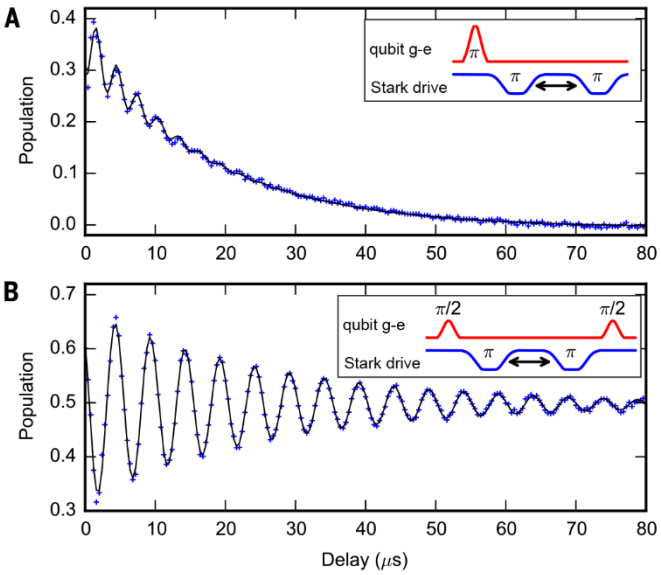

Fig. 4. Phonon coherence properties. (**A**) Phonon T_1 measurement. Black line is a fit to an exponential decay plus a decaying sinusoid. (**B**) Phonon T_2 measurement. The phase of the second $\pi/2$ pulse is set to be $(\omega_0 + \Omega)t$, where t is the delay, ω_0 is the detuning between the qubit and phonon during the delay, and Ω provides an additional artificial detuning. Black line is a fit to an exponentially decaying sinusoid with frequency Ω.

Downloaded from http://science.sciencemag.org/ on September 21, 2017

Science

Quantum acoustics with superconducting qubits

Yiwen Chu, Prashanta Kharel, William H. Renninger, Luke D. Burkhart, Luigi Frunzio, Peter T. Rakich and Robert J. Schoelkopf

published online September 21, 2017

ARTICLE TOOLS http://science.sciencemag.org/content/early/2017/09/20/science.aao1511

SUPPLEMENTARY MATERIALS http://science.sciencemag.org/content/suppl/2017/09/20/science.aao1511.DC1

REFERENCES This article cites 32 articles, 3 of which you can access for free
http://science.sciencemag.org/content/early/2017/09/20/science.aao1511#BIBL

PERMISSIONS http://www.sciencemag.org/help/reprints-and-permissions

Use of this article is subject to the Terms of Service

Science (print ISSN 0036-8075; online ISSN 1095-9203) is published by the American Association for the Advancement of Science, 1200 New York Avenue NW, Washington, DC 20005. 2017 © The Authors, some rights reserved; exclusive licensee American Association for the Advancement of Science. No claim to original U.S. Government Works. The title *Science* is a registered trademark of AAAS.

Downloaded from http://science.sciencemag.org/ on September 21, 2017